Journal of Power Sources 218 (2012) 148–156

Contents lists available at SciVerse ScienceDirect

Journal of Power Sources

journal homepage: www.elsevier.com/locate/jpowsour

Ni nanowire supported 3D flower-like Pd nanostructures as an efficient electrocatalyst for electrooxidation of ethanol in alkaline media

Maksudul Hasan [a], Simon B. Newcomb [b], James F. Rohan [a], Kafil M. Razeeb [a,*]

[a] Tyndall National Institute, University College Cork, Lee Maltings, Dyke Parade, Cork, Ireland
[b] Glebe Scientific Limited, Newport, Co. Tipperary, Ireland

HIGHLIGHTS

- Schematic of fabrication route for Pd nanoparticle or nanoflowers on Ni nanowire.
- Electron microscopy image of 3D flower-like Pd nano-electrocatalyst on Ni nanowires.
- Exhibits large active surface area and excellent electrocatalytic activity.
- The nano-heterostructure shows high level of the poisoning tolerance.

GRAPHICAL ABSTRACT

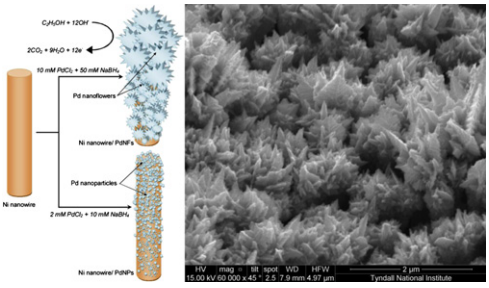

ARTICLE INFO

Article history:
Received 9 March 2012
Received in revised form
25 April 2012
Accepted 5 June 2012
Available online 3 July 2012

Keywords:
Pd nanoflowers
Electrocatalysts
Nanowire array
Catalysis
Direct ethanol fuel cells

ABSTRACT

A Ni nanowire array (NiNWA) supported three-dimensional flower-like Pd nano-electrocatalyst with high electrocatalytic performance for the electrooxidation of ethanol in alkaline media has been fabricated by borohydride hydrothermal reduction method. This novel hybrid NiNWA/PdNF (nanoflowers) electrocatalyst exhibits large electrochemically active surface area (EASA, 45 $m^2\,g^{-1}$(Pd)), excellent electrocatalytic activity (765 mA mg^{-1}(Pd)), and high level of the poisoning tolerance ($I_f/I_b = 1.2$) to the carbonaceous oxidative intermediates for the electrooxidation reaction in alkaline media. In addition, the electrochemical stability of NiNWA/PdNF is significantly higher than that of NiNWA/PdNP (nanoparticles) electrocatalyst, as evidenced by chronoamperometry experiments in which the electrooxidation current of nanoflowers is controlled by the diffusion transport of ethanol species rather than the carbonaceous poisoning. This high electrocatalytic activity can be attributed to the more open structure with higher electrochemically active sites and shape of Pd nanoflowers. This is further enhanced by the core support NiNWA with a very large surface area and the open interspaces that ensure easy alcohol access even to remote active sites for fast ion adsorption/desorption.

1. Introduction

Direct alcohol fuel cells (DAFCs) that directly convert the chemical energy stored in the alcohol into electricity are promising as power sources for auxiliary power in transportation, portable electronics, and other contemporary applications [1–4]. In particular, alkaline direct ethanol fuel cells (ADEFCs) have been the topic of numerous research papers [5–9]. This is due to the fact that ethanol is considered a most attractive liquid fuel with an energy density of 8 kWh kg^{-1} (cf. 6.1 kWh kg^{-1} for methanol) [10]. Large-scale production from the fermentation of biomass, ease of storage and transportation, and relative non-toxicity of ethanol and its final electrooxidation product CO_2 makes it an attractive fuel for ADEFCs [3,11]. Furthermore, during the electrocatalytic reactions in ADEFCs, the charge carrier is the anion (OH^-) instead of the proton (H^+), which avoid fuel crossover by electro-osmosis

* Corresponding author. Tel.: +353 21 4904078; fax: +353 21 4270271.
E-mail address: kafil.mahmood@tyndall.ie (K.M. Razeeb).

0378-7753/$ – see front matter © 2012 Elsevier B.V. All rights reserved.
http://dx.doi.org/10.1016/j.jpowsour.2012.06.017

drag of hydrated hydroxyl ions through the anion exchange membranes (AEMs) [12,13]. Finally, the electro-kinetics of both the ethanol oxidation reaction (EOR) [14–16] and oxygen reduction reaction (ORR) [17] are more facile in alkaline media than in acid media. Since non-precious metals are sufficiently stable in alkaline media, low cost Pt-free metals capable of efficient ethanol oxidation are expected to reduce the cost of ADEFCs [18]. The main pitfall associated with the alkaline fuel cells is the precipitation of carbonate salts on the electrode surface due to reaction with CO_2, the final product of ethanol electrooxidation. The carbonation of the aqueous electrolyte can be minimized by the application of AEMs as solid polymer electrolyte which also eliminates the electrolyte leakage [3,18]. Recently, novel AEMs modified by polymer electrolyte have shown excellent performance and stability in alkaline fuel cells [13,19]. However, further development and commercialization of the ethanol powered alkaline fuel cells is seriously hindered by two key issues—the slow kinetics or inefficient oxidation of ethanol to CO_2 caused by catalyst poisoning on available Pt-based electrocatalysts, and the cost of precious metals employed [2,20,21]. The development of electrocatalysts for ethanol oxidation to CO_2 that break the C–C bond has been a major challenge in electrocatalysis [18]. Nevertheless, it has shown recently that Pd is a more active, stable and poison tolerant electrocatalyst than Pt for ethanol oxidation in alkaline media [2,21–25]. Since Pd is cheaper and at least 50 times more earth abundant than Pt [21,26], it is promising for use as an electrocatalyst to replace Pt in ADEFCs. Notably, Pd nanostructures with high surface to volume ratio (e.g., nanowires [25], nanotubes [27], nanoporous[8] and nanoflowers [28]) have attracted much attention in fuel cell reactions.

Carbon nanotubes (CNTs) supported Pt nanoparticles (NPs) have demonstrated significant enhancement in electrocatalytic activity of fuel cells due to their higher electroactive surface area and stability than individual NP [29,30]. It is well understood that the performance of nanostructured electrocatalysts depends on their surface morphology (e.g., shape, size, etc.) and the supporting structures [28–30]. It has been demonstrated that CNTs supported flower-like Pt nanostructures shows high electrocatalytic performance compare to the commercial electrocatalyst [31]. Recently, three-dimensional flower-like Pd nanostructures have been shown to be more active and stable than their NP format for the electrooxidation of methanol in alkaline medium [28]. However, little efforts have been made in the fabrication of hybrid 3D flower-like Pd nanostructures [28,32]. Synthesis of hybrid nano-electrocatalyst on the walls of CNTs is still a challenge. CNTs are hydrophobic and usually require modification (e.g., inorganic acids used to generate carboxylic acid sites on the tube walls or polymer (surfactant) to functionalize) to facilitate their dispersion in water. Additionally, agglomeration of CNTs extensively reduces the surface area for the electrocatalysts support and increases the contact resistance [33]. On the other hand, nanowire or nanotube arrays have attracted increased attention due to their excellent physical and chemical properties [25,34–36]. The arrayed nanostructures possess a high electroactive surface area, allows fast diffusion of liquid alcohol, and useful ways to optimize and increase the utilization of precious metal electrocatalysts. Herein, we report a novel hybrid NiNWA/PdNF (nanoflowers) electrocatalyst using one-dimensional (1D) and conductive metal NiNWA as a support for the PdNF. This hybrid 3D PdNF electrocatalyst has been fabricated by electrodeposition of NiNWA using polycarbonate template and the reduction of Pd as NF onto the surface of NiNWA through borohydride hydrothermal reduction method. The results indicated that 3D flower-like NiNWA/PdNF electrocatalyst can be used as efficient electrocatalysts for ethanol electrooxidation in ADEFCs.

2. Experimental

2.1. Synthesis of NiNWA

Polycarbonate template (Isopore™ Membrane Filters of 47 mm diameter, pore diameter of ~220 nm, thickness of ~25–30 μm and porosity of ~13.8%) was purchased from Millipore Ireland B.V. The backside of the template was coated by a 400 nm thick layer of Ni using thermal evaporation technique (Temescal FC-2000). A copper wire was connected to the Ni backside of the template by silver paste (Radionics Ltd. Ireland) and dried overnight before use. Low stress nickel sulfamate bath was prepared using nickel sulfamate ($120\,g\,l^{-1}$), boric acid ($40\,g\,l^{-1}$), nickel bromide ($4\,g\,l^{-1}$) and wetting agent ANKOR (R) F ($10\,ml\,l^{-1}$). The pH of the solution was adjusted to 3.8 by adding 1 M sulfamic acid at room temperature. The solution was stirred slowly and the deposition was conducted at constant current ($50\,mA\,cm^{-2}$ as the ratio of the total template area) and temperature (50 °C). A two electrodes cell was used with Ni pellets in a Ti-basket as an anode and Ni/porous polycarbonate template as a cathode. The deposition rate of Ni nanowires was found to be 0.45 μm per minute. A thin film of Ni (3–4 μm) was also deposited onto the backside of the template which prevented nanowires from collapsing after the template dissolved in dichloromethane. The 1D NiNWA (~13 μm in length) was washed with plenty of deionized water and dried in air.

2.2. Synthesis of NiNWA supported PdNF

The NiNWA was cut into small pieces of $0.5 \times 0.5\,cm^2$ areas, cleaned in 1 M nitric acid for 1 min, washed repeatedly with deionized water and dried in air. The hybrid nano-electrocatalysts of NiNWA supported PdNF were prepared by a $NaBH_4$ hydrothermal reduction method from the chemical bath containing metal precursor salt (10 mM $PdCl_2$) in water. A piece of the NiNWA sample was immersed into a 5 ml glass tube contained 0.5 ml aliquots of Pd metal precursor salt at 80 °C, followed by stirring for 20 min. Subsequently, an excess quantity of freshly prepared $NaBH_4$ (10 mM) solution was added drop wise to the mixture and stirred slowly until its color turned from yellowish to colorless (typically 10 min required). The chemical reduction of Pd using the higher concentration metal precursor salt (10 mM $PdCl_2$) was illustrated as the vigorous reduction method. After completion of the reaction the resulting hybrid NiNWA/PdNF electrocatalyst was removed from the mixture and washed repeatedly with deionized water for the complete removal of residual Cl^- ions (the filtrate water was analyzed with 1 M silver nitrate solution and no white colored precipitate (AgCl) was obtained thereby confirming the complete removal of Cl^- ions). The PdNP were reduced onto the NiNWA surface using a similar technique but from the lower concentrations metal precursor salt (2 mM $PdCl_2$), which is referred to here as the mild reduction method. In this case, PdNP are formed instead of PdNF. The synthesized electrocatalysts were dried in an oven at 100 °C for 1.5 h. The amount of Pd reduced onto the surface of NiNWA was measured using a high precision electronic microbalance (Mettler Toledo, XS 105 Dual Range, repeatability (SD), $d = 0.01$ mg) from the weight difference before and after the reduction of Pd onto the surface of NiNWA support.

2.3. Structural and microscopic characterization

The morphology, nanostructure and particle size were acquired by scanning electron microscopy (SEM) (QUANTA FEG 650) coupled with energy dispersive X-ray spectroscopy (EDS Oxford Instruments INCA energy system) operating at an accelerating voltage of 200 kV. TEM images were obtained by using JEOL 2100 operated at

an accelerating voltage of 200 kV. Specimens for TEM examination were prepared by encapsulation in a low melting point wax and thinned to electron transparency using standard focused ion beam (FIB) thinning procedures described elsewhere [37]. X-ray diffraction (XRD) analysis was carried out with a Philips X'pert PW3710-MPD diffractometer using filtered Cu-Kα ($\lambda = 1.54$ Å) radiation, operated at 40 kV and 40 mA with a scan rate of 0.015 2θ/s.

2.4. Electrochemical characterization and ethanol electrooxidation

The electrocatalytic activities of the NiNWA/PdNF for the electrooxidation of ethanol were performed using a three-electrode electrochemical cell and a CH Instruments 660C potentiostat. Cyclic voltammetry (CV) and chronoamperometry (CA) were performed with the test cell filled with 1 M ethanol (EtOH) and 0.5 M KOH as an electrolyte, with platinized titanium mesh as the counter electrode and a Hg/HgO (1 M KOH solution) as the reference electrode. The working electrodes were the fabricated NiNWA/PdNP and NiNWA/PdNF. Each working electrode had an area of 0.5×0.5 cm^2. The electrochemical results are normalized to the electrochemically active surface area (EASA) of Pd. CV measurements were carried out in the potential range of 0.4 to −0.9 V at scan rates of 10–50 mV s^{-1} following conditioning at the open circuit potential (−0.55 V, OCP) for 20 s. CA measurements were carried out at a fixed potential of −0.2 V. The electrolyte was purged with N_2 for 30 min prior to each measurement and all experiments were conducted at room temperature 22 ± 1 °C.

3. Results and discussion

Fig. 1 shows SEM images of the NiNWA and NiNWA/PdNP electrocatalysts taken at 45° perspective view. Fig. 1(a) and highly magnified inset view clearly reveal the smooth surface of the as prepared nanowire arrays. Fig. 1(b) shows a little roughening of the surface morphology of the NiNWA after the reaction with metal precursor salt ($PdCl_2$) and $NaBH_4$ solution under the mild reduction condition. In the mild reduction method as mentioned in Section 2, using the lower concentration metal precursor salt, PdNP are found to be coated over the NiNWA walls. The point-resolved EDS spectra (see Fig. S-1 in the Supplementary Materials (SM)) collected at various points of the NiNWA/PdNP surface also confirm that NiNWA is well covered by PdNP, which are not visible in the EDS for the as prepared NiNWA (see Fig. S-2 in the SM). However, when Pd is deposited under the vigorous reduction condition using the higher concentration metal precursor salt, particles have the flower and budlike morphology, covered over the NiNWA surface or walls as shown in Fig. 2(a,b). The top of the NiNWA is fully covered with the PdNF (see Fig. 2(a)), but along the full length of the NiNWA homogeneous PdNP formed first as revealed by the high magnified view in Fig. 2(b), which is followed by the further growth of randomly and 3D interconnected nanoflowers network (see also TEM images in Fig. 3(a–c)). For disclosing the underlying fact that controls the formation of the PdNF with well-defined shape, different control experiments were performed by changing the amount of metal [Pd^{2+}] ions in precursor solution while other reaction parameters kept constant. We found that the morphology of the Pd deposits on the metallic NiNWA surface changes obviously when varying the amount of metal [Pd^{2+}] ions in the precursor solution. The increase in the amount of [Pd^{2+}] ions in precursor solution by applying either larger amount aliquots from a low molar concentration or smaller amount aliquots from a higher molar concentration leads to the more branching morphology of the Pd deposit. As for example, when an intermediate concentration metal precursor (5 mM) was used at the similar reaction condition, a smaller budlike morphology of the Pd was

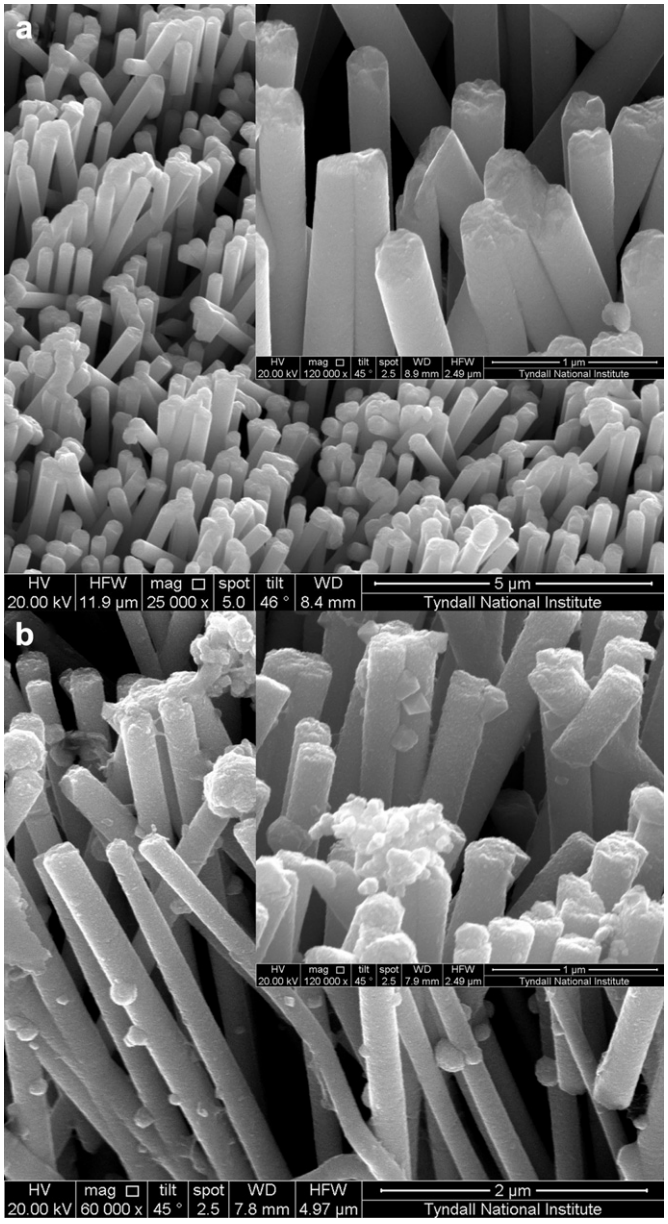

Fig. 1. SEM images (a) NiNWA top view, and (b) NiNWA supported Pd nanoparticles cross-sectional view. Insets are the corresponding high magnified top views, inset of (b) showing that PdNP have been coated around the circumference of NiNWA.

developed (see Fig. S-3 in the SM). However, there were nanoparticles and well-defined flower-like morphology at lower (2 mM) and higher (10 mM) metal precursor concentration, respectively. Hence, the different concentrations of metal precursor salt leads to the different shape and morphological changes in the final structure, and high precursor concentration is favorable for the formation of a highly branched morphology [28,38]. Fig. S-4 in the SM shows the point-resolved EDS spectra of NiNWA/PdNF, in which Pd counts are much higher by comparison with the Pd count in the case of mild reduction method (which resulted in PdNP coverage) (see Fig. S-1 in the SM). The composition of these electrocatalysts is extracted from the EDS elemental analysis, where Ni and Pd ratios are approximately 0.7:1 (38.92 wt% Ni, 54.64 wt% Pd, 6.44 wt% C) for NiNWA/PdNF and 9:1 (89.88 wt% Ni, 9.96 wt% Pd, 0.16 wt% C) for NiNWA/PdNP, showing the presence of a large quantity of Pd in the nanoflowers by comparison with the nanoparticles sample. Further

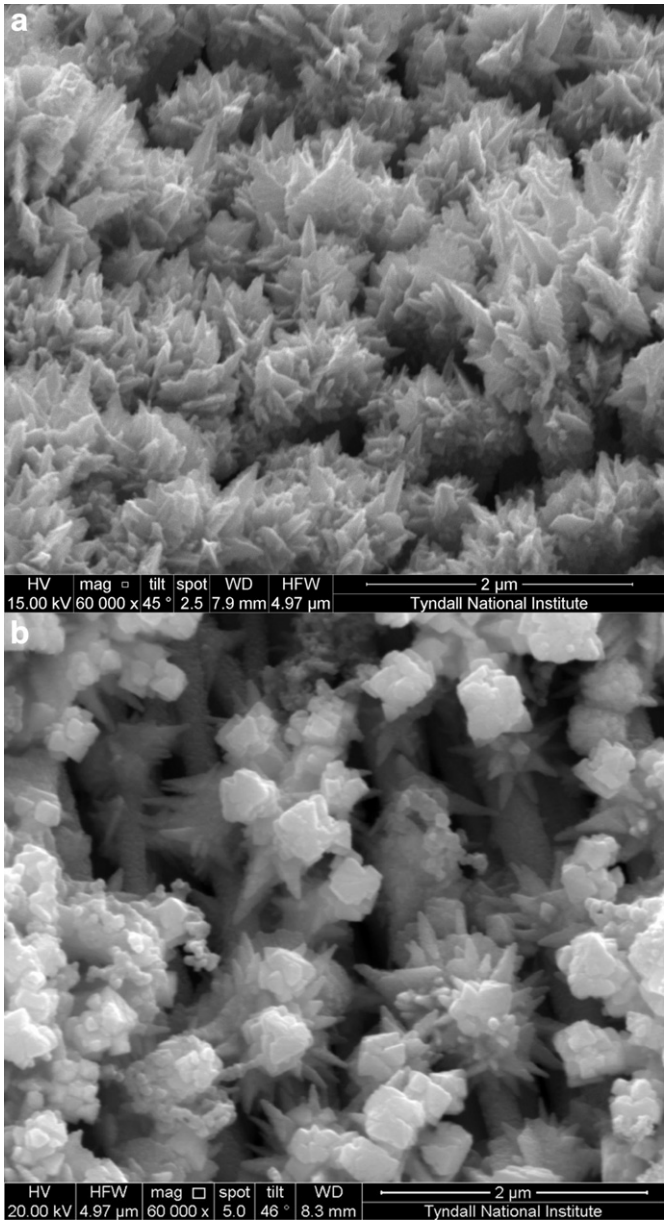

Fig. 2. SEM images of NiNWA supported PdNF show (a) top view, (b) high magnified cross-sectional view. The highly magnified cross-sectional view shows that the walls of the NiNWA are coated with PdNP, which is followed by the further growth toward PdNF.

insight into the microstructure of the PdNF formed at the surfaces of NiNWA is obtained by TEM measurements. Fig. 3 shows the bright field (BF) TEM images and SAED taken from the sample NiNWA/PdNF. Fig. 3(a,b) shows the region of the extended Pd growth toward flower at increasing magnification, and the thickness of the PdNF is locally as high as ~400 nm. PdNP are formed at the walls of Ni nanowire as can be seen from the cross-section BF TEM image in Fig. 3(c), which has a variable thickness of 50–100 nm. The diffraction pattern shown in Fig. 3(d) was obtained from a typical region of the PdNF shown in Fig. 3(a,b) and demonstrates the presence of face-centered cubic (fcc) Pd for which the measured (111), (200), (220) and (311) d-spacings are 0.223, 0.194, 0.137 and 0.117 nm, respectively. The PdNF was found to have a generally coarse grained microstructure and to contain twins. The deposit is well adhered to the Ni surface and has a distribution of relatively fine grains (~25–50 nm). The XRD patterns in Fig. 4 clearly indicate that the hybrid NiNWA/PdNP and NiNWA/PdNF electrocatalysts have face-centered cubic (fcc) structures. Sharp and well-defined peaks are observed for Pd at 2θ values of 40.07, 46.59, 68.08, and 82.10° corresponding to planes of (111), (200), (220), and (311), respectively, according to JCPDS No. 05-0681. The full-width at half maximum (FWHM) of the plane (111) is used to calculate the average crystal size of the PdNF and PdNP by Debye–Scherrer equation ($B_{2\theta} = 0.94\lambda/r\cos\theta$, where $B_{2\theta}$ is FWHM, λ incident wavelength, r is the crystallite diameter, and θ is the diffraction angle). The average crystallite sizes are 21.8 nm and 7.2 nm for the nanoflowers and nanoparticles, respectively. The XRD pattern is consistent with selected area electron diffraction (SAED) in Fig. 3(d), which confirms the polycrystalline nature of the Pd and the localized TEM analysis showed a distribution of relatively fine Pd grains (~25–50 nm).

Typical cyclic voltammograms of NiNWA, NiNWA/PdNP, and 3D flower-like NiNWA/PdNF electrocatalysts in 0.5 M KOH are shown in Fig. 5. The characteristic features of hydrogen adsorption/desorption, double-layer charging and oxide formation/reduction are evident from the voltammetric profile of the Pd-based electrocatalysts. However, no electrocatalytic activity is noticeable for the bare NiNWA apart from the hydrogen evolution at potentials more negative than −0.9 V with a limited capacitance response (6.5 mF cm^{-2}) before the oxygen evolution reaction (0.1–0.4 V) [39]. The real electrochemically active surface area (EASA) of the electrocatalysts can be obtained from the cyclic voltammograms using the following equation [5,9,40].

$$\text{EASA} = \frac{Q_H}{Q_M} \quad (1)$$

where Q_M is the charge due to the monolayer adsorption of hydrogen (mC cm^{-2} for Pd) onto the electrode and Q_H is the charge (mC) due to hydrogen absorption determined experimentally. The peak in the potential region of −0.9 V to −0.4 V in the cathodic scan is due to a monolayer adsorption of hydrogen onto the Pd surface followed by the emergence of the hydrogen evolution reaction beyond −0.9. In alkaline solution, the concentration of hydrogen ions [H^+] is negligible and therefore, the hydrogen evolution reaction proceeds through the discharge of a water molecule (Eq. (2)) to yield adsorbed atomic hydrogen on the metal (Pd) surface and the removal of this adsorbed atomic hydrogen from the surface could proceed by recombination (Eq. (3)) [41].

$$H_2O + Pd + e^- \leftrightarrow Pd - H_{ads} + OH^- \quad (2)$$

$$Pd - H_{ads} + Pd - H_{ads} \leftrightarrow H_2 + 2Pd \quad (3)$$

The peaks in the potential region of −0.9 V to −0.4 V in the anodic scan corresponds to the electrochemical desorption of chemisorbed monolayer hydrogen, which is also known as the electrooxidation of hydrogen as expressed by the following equation [42–44].

$$Pd - H_{ads} + OH^- \leftrightarrow Pd + H_2O + e^- \quad (4)$$

The charge associated with the formation of a hydrogen monolayer for Pt is considered to be 0.21 mC cm^{-2} after double-layer correction [40]. For Pd-based electrocatalysts, the measured EASA value using this method (Eq. (1)) can be less precise due to excess hydrogen absorption by comparison with Pt (Pd is a good H_2 storage material). Therefore, the real EASA value was also calculated from the Columbic charge associated with the reduction of palladium oxide (PdO) determined from the peak centered at −0.2 V (cathodic), which has been formed on the Pd surface during the

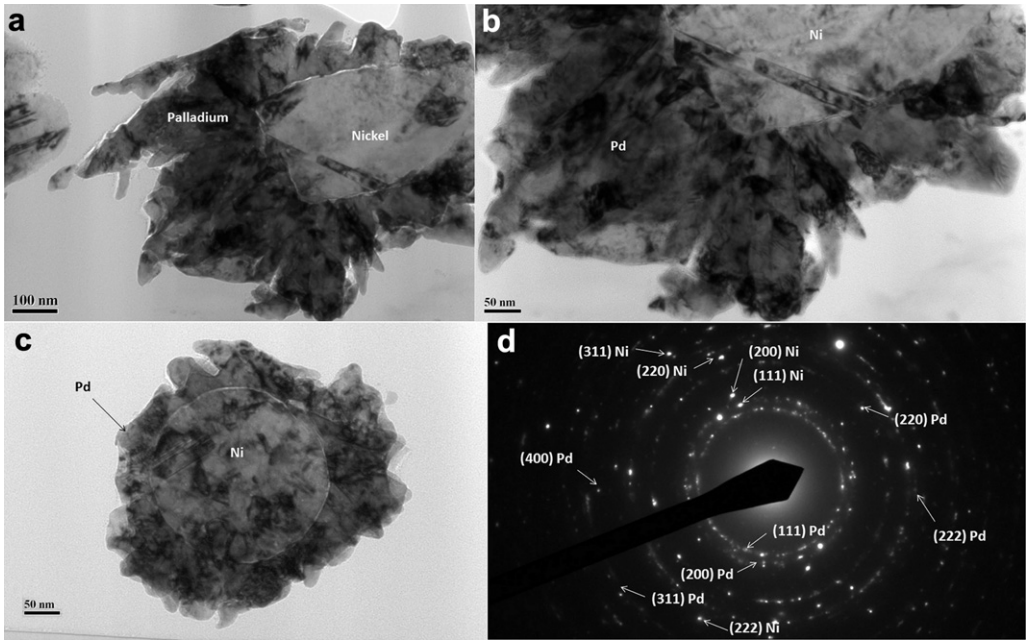

Fig. 3. BF TEM images of transverse cross-section showing (a) PdNF at the surface of a Ni nanowire, (b) high magnification region of (a), and (c) a full coverage of Pd that varies in thickness from ~50 to 100 nm. (d) A diffraction pattern confirming the presence of Ni and Pd, and the lattice parameter of the fcc Pd is found to be approximately 0.3944 nm.

anodic scan [45]. The formation of the palladium oxide (PdO) layer in the anodic scan involves the chemisorption of OH^- on the Pd surface starting above −0.2 V, which is then transformed into higher valence oxides at higher potentials as defined by the following equations [42,44,46].

$$Pd + OH^- \leftrightarrow Pd - OH_{ads} + e^- \quad (5)$$

$$Pd - OH_{ads} + OH^- \leftrightarrow Pd - O + H_2O + e^- \quad (6)$$

$$Pd - OH_{ads} + Pd - OH_{ads} \leftrightarrow Pd - O + H_2O \quad (7)$$

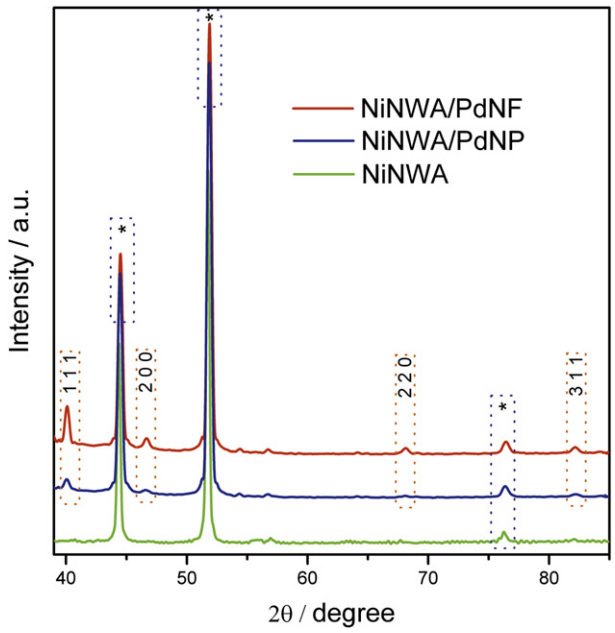

Fig. 4. XRD patterns of the as electrodeposited NiNWA, NiNWA/PdNP, and NiNWA/PdNF. The peaks marked by asterisks correspond to the metallic Ni phases.

The consequent reduction process of the associated PdO during the cathodic scan (centered at −0.2 V) can be described by Eq. (8) [42–44,46].

$$Pd - O + H_2O + 2e^- \leftrightarrow Pd + 2OH^- \quad (8)$$

The charge required for the reduction of PdO monolayer is assumed to be 0.405 mC cm^{-2} as reported previously [47]. Therefore, the EASA of the Pd-based nanoelectrode catalysts has been measured by the following equation [48].

$$EASA = \frac{Q_R}{Q_{MR}} \quad (9)$$

where Q_R is the columbic charge required for the PdO reduction (mC), Q_{MR} is the charge for the reduction of the PdO monolayer (0.405 mC cm^{-2} for Pd). The values of the EASA calculated using

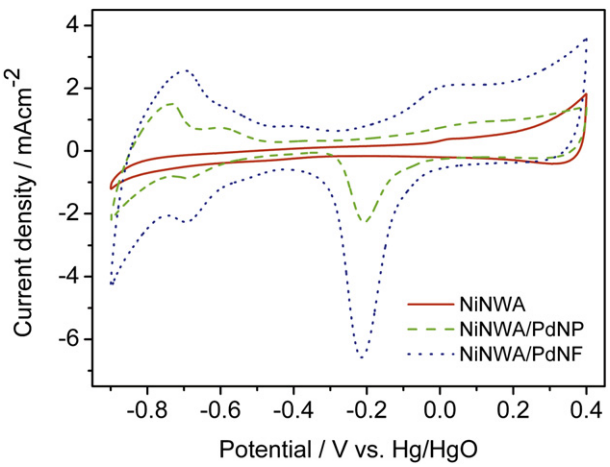

Fig. 5. Cyclic voltammograms of NiNWA, NiNWA/PdNP, NiNWA/PdNF in 0.5 M KOH solution. Conditioning/initial potential: −0.5 V, 20 s; scan rate: 50 mV s^{-1}. Here, voltammetric currents are expressed in terms of the geometrical surface area of the electrode.

both Eqs. (1) and (9), are summarized in Table 1. It can be seen from the Table 1 that the oxide method leads to slightly lower values of EASA than determined from the monolayer hydrogen adsorption/desorption method described above. Using the values determined from the oxide reduction, the EASA of PdNF is much higher than that of the PdNP electrocatalyst. The EASA of NiNWA/PdNF (45 $m^2 g^{-1}$(Pd)) is ~2 times higher than that of NiNWA/PdNP (21.5 $m^2 g^{-1}$(Pd)), which suggests higher utilization efficiency of Pd in the nanoflowers structure. This is most likely due to the abundant grain boundaries and the three-dimensional open nanostructure of the PdNF, which enhances the accessibility of ethanol to the active sites for electrooxidation.

The electrocatalytic activity of NiNWA/PdNF for the electrooxidation reaction of ethanol has been studied using cyclic voltammetry. Fig. 6(a) shows the quasi-steady-state cyclic voltammograms of NiNWA/PdNP and NiNWA/PdNF electrocatalysts in 0.5 M KOH solution containing 1 M ethanol. Ethanol electrooxidation is characterized by two well-defined anodic current peaks. One is in the forward scan (i.e., under anodic condition) at 0.075 V vs. Hg/HgO and the other one on the reverse scan (i.e., under cathodic condition) at −0.17 V. This is typical of ethanol electrooxidation on Pd-based electrocatalysts, which exhibits a double electrooxidation peak [15,25,28,35]. The oxidation current peak in the forward scan is due to the electrooxidation of the freshly chemisorbed ethanol species onto the Pd catalyst, and the peak in the backward scan is primarily caused by the oxidation of intermediates of alcohol dissociative adsorption [49]. The hydrogen adsorption/desorption reaction (−0.9 V to −0.4 V) is significantly suppressed in the ethanol contained solution (see Fig. 6(b)). The suppression of the reactions in the hydrogen region can be accredited to the dissociative adsorption of ethanol at the low potential region (−0.9 V to −0.4 V) as described by the Eqs. (10) and (11) [44].

$$Pd + CH_3CH_2OH \leftrightarrow Pd - (CH_3CH_2OH)_{ads} \quad (10)$$

$$Pd - (CH_3CH_2OH)_{ads} + 3OH^- \leftrightarrow Pd - (CH_3CO)_{ads} + 3H_2O + 3e^- \quad (11)$$

It can be seen from the above Eqs. (10) and (11) that the adsorbed acyl group ($(CH_3CO)_{ads}$), onto the active sites of the Pd electrocatalyst inhibits the adsorption/desorption of hydrogen, thereby suppressing the hydrogen peaks. The onset anodic potential (E_{op}) for the ethanol electrooxidation on the NiNWA/PdNF is −0.6 V, well above the starting potential for the adsorption of the hydroxyl (OH^-) ions (Eq. (5)), which is 100 mV more negative than that of the NiNWA/PdNP ($E_{op} = -0.5$ V) (see inset Fig. 6(a)). This fact implies that the PdNF enhance the stripping reaction of the adsorbed intermediates, which are formed during the dissociative adsorption of ethanol, by the adsorbed hydroxyl species (Pd-OH_{ads}) (Eq. (12)). This stripping reaction is the rate-determining step for the electrooxidation of ethanol on Pd electrocatalyst in alkaline solution, as discussed later. The first three cyclic voltammograms for the electrooxidation of ethanol on freshly prepared NiNWA/PdNF are shown in Fig S-5 in the SM section. It can be seen that the onset anodic potential for the three cycles is similar at −0.6 V but a little anodic peak potential shift (25 mV) toward the negative direction is observed after the first cycle. The peak potential shift toward a more negative value suggests that the electrode shows some resistance in the first cycle, which is probably caused by the electrode contaminants incorporated during the fabrication process. The electrochemically active sites are activated evenly on the repeated cycling and voltammograms became quasi-steady-state.

Table 1
Results of the voltammetric analysis of the NiNWA supported Pd nanoparticles and nanoflowers electrocatalysts.

Electrocatalysts	EASA ($m^2 g^{-1}$(Pd))		Onset	Pd-specific	Pd mass
	H_2 ads/des	Red. of ads O_2	Potential (V)	Activity (mA cm^{-2}(Pd))	Activity (mA mg^{-1}(Pd))
NiNWA/PdNP	30	21.5	−0.5	0.15	32
NiNWA/PdNF	52	45	−0.6	1.7	765

Results of the voltammetric analysis of the NiNWA supported Pd nanoparticles and nanoflowers electrocatalysts. Specific activity has been normalized to the electrochemically active surface area (EASA) of Pd.

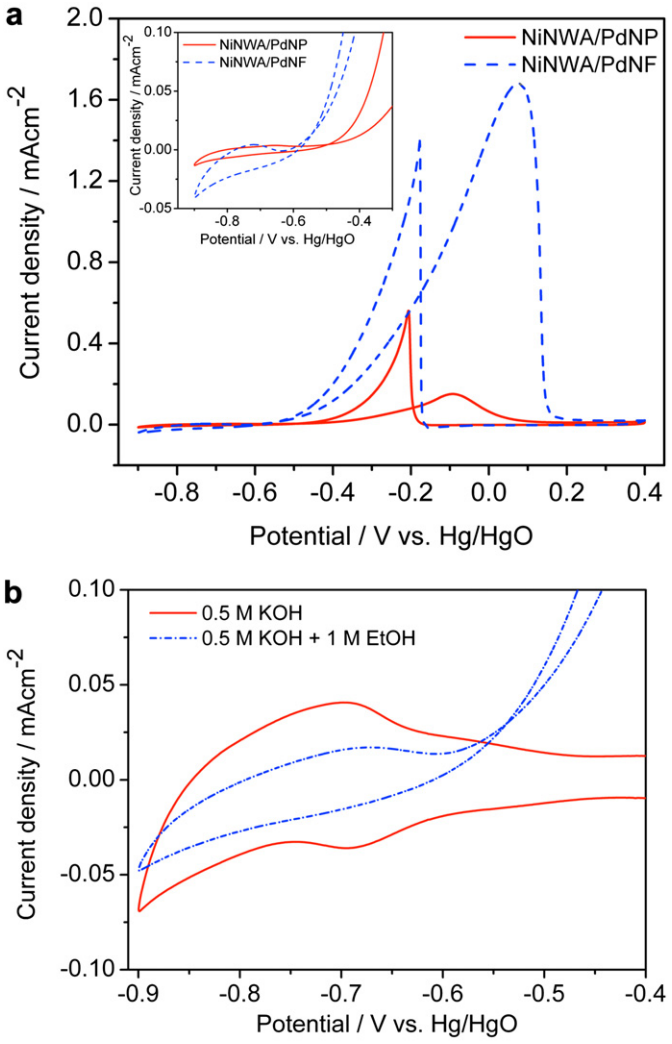

Fig. 6. (a) Cyclic voltammograms of NiNWA/PdNP and NiNWA/PdNF for the electrooxidation of ethanol in 0.5 M KOH + 1 M EtOH solution. Conditioning/initial potential: −0.55 V, 20 s; scan rate: 20 mV s^{-1}, (b) Cyclic voltammograms of NiNWA/PdNF in 0.5 M KOH solution, and in 0.5 M KOH + 1 M EtOH solution in the hydrogen adsorption/desorption region (scan rate: 50 mV s^{-1}). Inset shows the magnified view of onset potential region of cyclic voltammograms.

The anodic peak current density (specific activity) of the PdNF, 1.7 mA cm^{-2} at the peak position of 0.075 V, is much higher than that of the PdNP (0.15 mA cm^{-2} at peak position −0.09 V), which indicates that the PdNF has excellent electrocatalytic activity for ethanol electrooxidation. The Pd loading in the electrocatalysts shown in Fig. 6(a) is 0.06 mg cm^{-2}, and 0.14 mg cm^{-2} for NiNWA/PdNP and NiNWA/PdNF electrodes, respectively. The Pd loading in the 3D flower-like NiNWA/PdNF is about ~2 times higher than in the NiNWA/PdNP electrocatalyst but the specific electrocatalytic activity has been increased by ~10 times, which implied that

precious Pd catalyst have higher utilization efficiency in the nanoflowers than in the nanoparticles structure. The high electrocatalytic performance of NiNWA/PdNF electrocatalyst is mainly due to the inherent nature of the abundant grain boundaries and the three-dimensional open nanostructure of the flowers that inhibits the undesirable agglomeration of the active sites [38,50]. It is interesting to note that the specific electrocatalytic activity of the NiNWA/PdNF (1.7 mA cm^{-2}, normalized to EASA) electrocatalyst is much higher than the corresponding activity reported for the commercial Pd/C (0.17 mA cm^{-2}, normalized to EASA) [51]. The Pd mass activity of the NiNWA/PdNF electrocatalyst is calculated to be 765 mA mg^{-1}(Pd), which is ~24 times higher than the NiNWA/PdNP (32 mA mg^{-1}(Pd)). A comparison cyclic voltammetry study for the electrooxidation of ethanol on Pd electrocatalyst with different morphology is shown in the SM section (Fig. S-6 and Table S-1). It clearly shows that mass activity of the electrocatalysts increases as the morphology changes from nanoparticles to a more bud-like/flower-like branched nanostructure. This high mass activity can be attributed to the interconnected PdNF with the large EASA that have been supported on a highly conductive and robust Ni metallic core. Additionally, the core support NiNWA has a very large surface area and the open interspaces ensure easy alcohol access even to remote active sites for fast ion adsorption/desorption.

The ratio of the forward anodic peak current density (I_f) to the backward anodic peak current density (I_b) is commonly used to characterize the tolerance to carbonaceous oxidative intermediates accumulation on the electrocatalyst surface. A high I_f/I_b ratio implies effective oxidation of ethanol to the end products during the anodic scan, and low accumulation and/or effective removal of the poisoning species on/from the electrocatalyst surface [49]. For, NiNWA/PdNF, the I_f/I_b value is 1.2 ($I_f = 1.7$ mA, $I_b = 1.4$ mA), which is ~5 times higher than for NiNWA/PdNP (~0.25, $I_f = 0.15$ mA, $I_b = 0.56$ mA). Since the commercial Pt/C NP electrocatalysts have an I_f/I_b value of 0.76 [52], the value (1.2) obtained in NiNWA/PdNF is ascribed to the nanoflowers morphology of Pd electrocatalyst. This result implies that more carbonaceous intermediates are being oxidized effectively on the nanoflowers surface during the forward scan, which is an indication of the nanoflowers' greater poisoning tolerance to carbonaceous oxidative intermediates.

To understand the nature of the mass transport behavior of the PdNF electrocatalyst, a series of cyclic voltammograms have been recorded at different scan rates. The CVs of the NiNWA/PdNF at different scan rates in Fig. 7(a) indicate that the electrooxidation peak current (anodic) density increases with the scan rates. The anodic peak current densities in the forward scan (at different scan rates) illustrate a linear relationship with the corresponding electrooxidation peak potential (see Fig. 7(b)), indicating that electrocatalytic process for the ethanol electrooxidation is controlled by the mass transport or the concentration polarization [28]. Fig. S-7 in the SM shows the relationship between the anodic peak current density and the square root of the scan rate for NiNWA/PdNP and NiNWA/PdNF electrodes. Both electrodes show a linear relationship with the scan rates, which further supported the mass transport controlled electrooxidation reactions of ethanol. These results suggest that 3D flower-like NiNWA/PdNF can be a useful electrocatalyst in ADEFCs. However, the integrated charge of the forward anodic peak for the ethanol electrooxidation decreases with increasing scan rate, as shown in Fig. S-8 (see in the SM). Therefore, the mass transport process both for the nanoparticles and flower-like Pd electrocatalysts is hindered at higher scan rate in the electrooxidation reactions of ethanol. The electrochemical hindrance in mass transport at higher scan rate is due to the difficulty in achieving full utilization of the electrode surface for these very high surface area electrocatalysts [2,35].

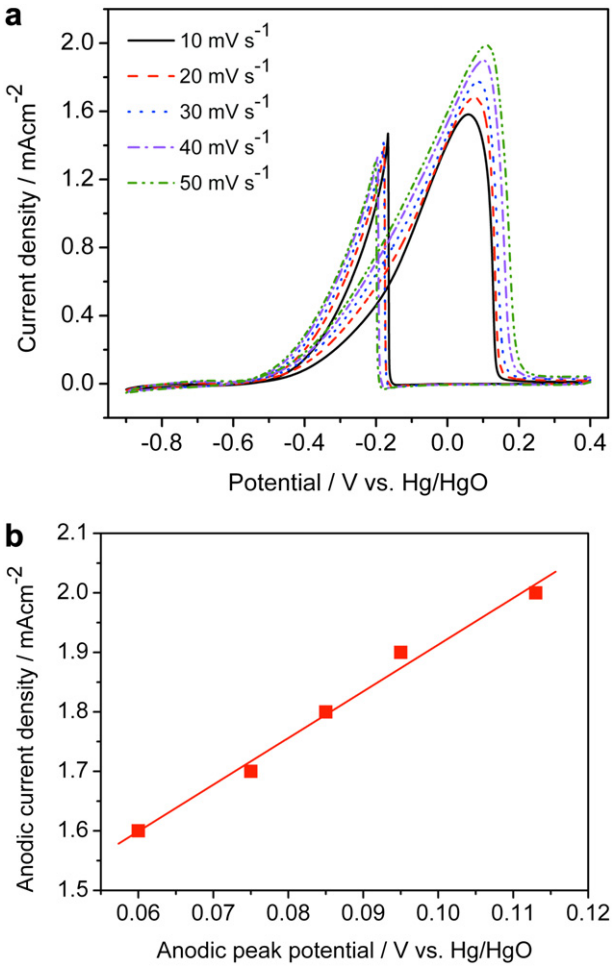

Fig. 7. (a) Cyclic voltammograms of NiNWA/PdNF for the electrooxidation of ethanol at different scan rates in 0.5 M KOH + 1 M EtOH solution, (b) Plot of forward anodic peak current density and the corresponding peak potential at different scan rates.

In order to understand the electrooxidation products of ethanol on NiNWA/PdNF, cyclic voltammograms have been recorded in 1 M KOH solution containing three fuels—ethanol, acetaldehyde and potassium acetate. The CVs of the NiNWA/PdNF in three different fuels in Fig. 8 showed that the peak current electrocatalytic activity for the electrooxidation of acetaldehyde (1.5 mA cm^{-2}) is slightly lower than that of the ethanol (1.7 mA cm^{-2}), while no electrooxidation current of the acetate is obtained. This finding implies that acetaldehyde is a major active intermediate that being converted to the acetate as the final product during the electrooxidation of ethanol on Pd electrocatalyst, which is also consistent with recent investigations [15,44]. The chemoselectivity for the electrooxidation of ethanol on Pd electrocatalyst has recently been investigated using in *situ* FTIR spectroscopy at different pH values [53]. It has been suggested that the acetate is the main product in the moderate concentrations of alkaline solution (≥0.5 M, pH = 14), while the formation of CO_2 due to the oxidative cleavage of C–C bond is obtained for pH values equal to or lower than 13. Therefore, due to the similar electrocatalytic activity of ethanol and acetaldehyde in this study, potassium acetate is the main byproduct for the electrooxidation of ethanol on NiNWA/PdNF in 0.5 M alkaline solution (pH = 14). It has also been suggested that the rate-determining step is the stripping of the adsorbed acyl intermediate by the adsorbed hydroxyl (Eq. (12)).

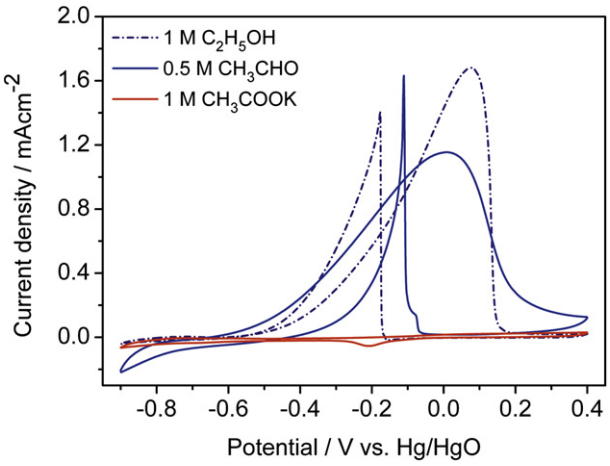

Fig. 8. Cyclic voltammograms of NiNWA/PdNF for the electrooxidation of ethanol in 0.5 M KOH solution containing three fuels: ethanol, acetaldehyde and potassium acetate. Conditioning/initial potential: −0.55 V, 20 s; scan rate: 20 mV s^{-1}.

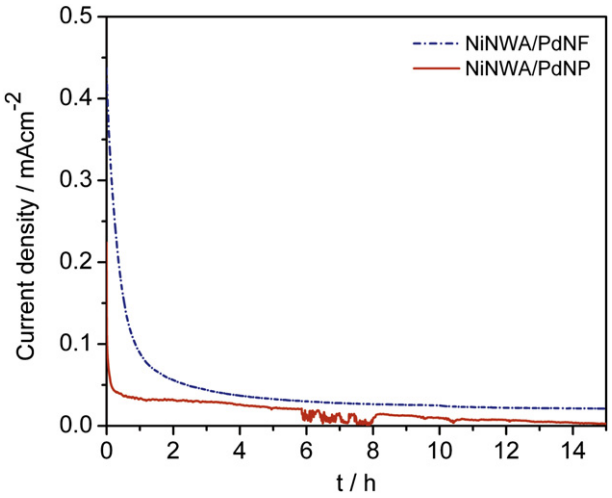

Fig. 10. Chronoamperograms for the electrooxidation of ethanol on NiNWA/PdNP and NiNWA/PdNF at −0.2 V (vs. Hg/HgO) in 0.5 M KOH + 1 M EtOH solution.

$$Pd - (CH_3CO)_{ads} + Pd - OH_{ads} \leftrightarrow Pd - CH_3COOH + Pd \quad (12)$$

$$Pd - CH_3COOH + OH^- \leftrightarrow Pd + CH_3COO^- + H_2O \quad (13)$$

Tafel plots of the electrooxidation of ethanol on NiNWA/PdNP and NiNWA/PdNF electrodes, derived from the cyclic voltammograms in 0.5 M KOH and 1 M EtOH solution at a scan rate of 2 mV s^{-1} (quasi-steady-state), are shown in Fig. 9. The similarity in the Tafel slopes suggest similar reaction mechanism for both electrocatalysts, and the lowest value obtained for NiNWA/PdNF (96 mV dec^{-1}) indicates a higher charge transfer rate during the electrooxidation of ethanol by comparison with the NiNWA/Pd electrocatalyst (118 mV dec^{-1}). Tafel slopes on both electrocatalysts are good agreement with the Temkin-type adsorption both for hydroxyl (OH_{ads}^-) and acyl (CH_3CO_{ads}) at low potential (charge transfer control region), suggesting that the stripping reaction (Eq. (12)) is the rate-determining step [44,54,55].

The electrochemical stability of NiNWA/PdNF for the electrooxidation of ethanol have been further investigated by chronoamperometry experiments at a fixed potential −0.2 V (vs. Hg/HgO), and the obtained result is compared with that of NiNWA/PdNP as shown in Fig. 10. The high current observed in the initial stage is due to the double-layer charging and this is more pronounced in the nanoflowers compare to nanoparticles electrode. The polarization current decayed sharply for the NiNWA/PdNP, but is more gradual for the NiNWA/PdNF electrocatalyst. The decrease in the polarization current with the increase in polarization time is due to the combination of electrocatalyst poisoning by the chemisorbed carbonaceous oxidative intermediates and the concentration polarization with time. The limited mass transport can have significant effects in the decay of electrooxidation current with increasing reaction time. Fig. S-9 in the SM shows the effect of depleting electroactive species near the surface of the electrocatalysts with increase in electrooxidation time, in which nanoflowers exhibit a linear relationship between electrooxidation current and the inverse square root of time by comparison with nanoparticles electrode. Therefore, the decay of the polarization current (Fig. 10) of NiNWA/PdNF electrocatalyst is mostly associated with the diffusion-controlled transport of ethanol species to the higher active surface area of nanoflowers. The current fluctuation appears during the electrooxidation of ethanol on the NiNWA/PdNP at relatively long time test, which is a typical phenomenon of a poisoned electrocatalyst. Conversely, the electrooxidation of ethanol on the NiNWA/PdNF is more stable at the long time period examined and no fluctuation is observed in the polarization current. At the end of total 15 h test, the electrooxidation current density on the NiNWA/PdNF (0.025 mA cm^{-2}) is ~12 times higher than that on the NiNWA/PdNP (0.002 mA cm^{-2}) electrocatalyst. It can be seen that the current density for NiNWA/PdNF after 15 h stability test is ~6% of the initial value whereas, this current density is only ~2% for NiNWA/PdNP electrocatalyst. The results show that NiNWA supported three-dimensional flower-like Pd nanostructures is more stable, efficient and poisoning tolerant electrocatalyst for the electrooxidation reaction in alkaline media.

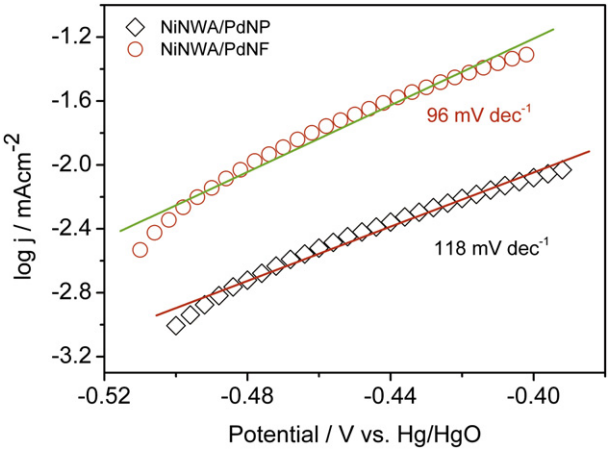

Fig. 9. Tafel plots for the electrooxidation of ethanol on NiNWA/PdNP and NiNWA/PdNF electrocatalyst in 0.5 M KOH + 1 M EtOH solution at lower potential region.

4. Conclusions

We have demonstrated a facile and cost effective method to fabricate Ni nanowire array supported three-dimensional flower-like Pd nano-electrocatalyst and investigated their electrocatalytic performance toward electrooxidation reaction in alkaline media. It has been shown that 1D metallic Ni nanowire array can be used as a noble metal catalyst supports as an alternative to CNTs. The novel hybrid Ni nanowire array/Pd nanoflowers electrocatalyst exhibits large electrochemically active surface area (EASA), excellent

electrocatalytic activity, and higher levels of stability and poisoning tolerance than Pd nanoparticles for the electrooxidation reactions of ethanol in alkaline media. This high electrocatalytic activity can be attributed to the inherent nature of the abundant grain boundaries and the three-dimensional open nanostructure of the Pd nanoflowers. The open interspaces of the highly conductive and robust Ni metallic core ensure significant alcohol access even to the remote active sites of the electrocatalyst for fast ion adsorption/desorption. The three-dimensional flower-like nanostructures of Pd with the highly branched shape and interspaces have been significant in achieving the outstanding electrocatalytic performance and pave the way for its use as an efficient electrocatalyst for Pt-free ADEFCs.

Acknowledgments

This work is financially supported by Enterprise Ireland (EI) under the commercialization fund CFTD/2008/322.

Appendix A. Supplementary material

Supplementary material (EDS of NiNWA, NiNWA/PdNP and NiNWA/PdNF, SEM of the smaller budlike Pd nanostructure, CVs of the Pd electrocatalysts with various morphology, plot of forward anodic peak current density vs. square root of the scan rate, plot of normalized charge of the forward anodic peak vs. scan rates, and plot of chronoamperometric current vs. inverse square root of the time for NiNWA/PdNP and NiNWA/PdNF electrocatalysts) is available in the online version of this article at http://dx.doi.org/10.1016/j.jpowsour.2012.06.017

References

[1] C. Lamy, A. Lima, V. LeRhun, F. Delime, C. Coutanceau, J.M. Leger, Journal of Power Sources 105 (2002) 283–296.
[2] E. Antolini, Journal of Power Sources 170 (2007) 1–12.
[3] C. Bianchini, P.K. Shen, Chemical Reviews 109 (2009) 4183–4206.
[4] A. Verma, S. Basu, Journal of Power Sources 145 (2005) 282–285.
[5] J. Datta, A. Dutta, S. Mukherjee, Journal of Physical Chemistry C 115 (2011) 15324–15334.
[6] C. Mahendiran, T. Maiyalagan, K. Scott, A. Gedanken, Materials Chemistry and Physics 128 (2011) 341–347.
[7] M.C. Oliveira, R. Rego, L.S. Fernandes, P.B. Tavares, Journal of Power Sources 196 (2011) 6092–6098.
[8] X. Xing, S. Cherevko, C.-H. Chung, Materials Chemistry and Physics 126 (2011) 36–40.
[9] H.L. Gao, S.J. Liao, Z.X. Liang, H.G. Liang, F. Luoa, Journal of Power Sources 196 (2011) 6138–6143.
[10] W.J. Zhou, S.Q. Song, W.Z. Li, Z.H. Zhou, G.Q. Sun, Q. Xin, S. Douvartzides, P. Tsiakaras, Journal of Power Sources 140 (2005) 50–58.
[11] A.E. Farrell, R.J. Plevin, B.T. Turner, A.D. Jones, M. O'Hare, D.M. Kammen, Science 311 (2006) 506–508.
[12] L. Li, Y.X. Wang, Journal of Membrane Science 262 (2005) 1–4.
[13] H.Y. Hou, S.L. Wang, W. Jin, Q. Jiang, L.L. Sun, L.H. Jiang, G.Q. Sun, International Journal of Hydrogen Energy 36 (2011) 5104–5109.
[14] C.W. Xu, L.Q. Cheng, P.K. Shen, Y.L. Liu, Electrochemistry Communications 9 (2007) 997–1001.
[15] H. Liu, J. Ye, C. Xu, S.P. Jiang, Y. Tong, Electrochemistry Communications 9 (2007) 2334–2339.
[16] G.F. Cui, S.Q. Song, P.K. Shen, A. Kowal, C. Bianchini, Journal of Physical Chemistry C 113 (2009) 15639–15642.
[17] L. Jiang, A. Hsu, D. Chu, R. Chen, Journal of Electrochemical Society 156 (2009) B643–B649.
[18] E.H. Yu, U. Krewer, K. Scott, Energies 3 (2010) 1499–1528.
[19] J.R. Varcoe, R.C.T. Slade, E. Lam How Yee, Chemical Communications (2006) 1428–1429.
[20] C. Lamy, S. Rousseau, E.M. Belgsir, C. Coutanceau, J.M. Leger, Electrochimica Acta 49 (2004) 3901–3908.
[21] E. Antolini, Energy & Environmental Science 2 (2009) 915–931.
[22] C.W. Xu, P.K. Shen, Y.L. Liu, Journal of Power Sources 164 (2007) 527–531.
[23] H.T. Zheng, Y.L. Li, S.X. Chen, P.K. Shen, Journal of Power Sources 163 (2006) 371–375.
[24] F. Hu, C. Chen, Z. Wang, G. Wei, P.K. Shen, Electrochimica Acta 52 (2006) 1087–1091.
[25] C.W. Xu, H. Wang, P.K. Shen, S.P. Jiang, Advanced Materials 19 (2007) 4256.
[26] O. Savadogo, K. Lee, K. Oishi, S. Mitsushima, N. Kamiya, K.I. Ota, Electrochemistry Communications 6 (2004) 105–109.
[27] Z.W. Chen, M. Waje, W.Z. Li, Y.S. Yan, Angewandte Chemie International Edition 46 (2007) 4060–4063.
[28] Z. Yin, H.J. Zheng, D. Ma, X.H. Bao, Journal of Physical Chemistry C 113 (2009) 1001–1005.
[29] L.Q. Hoa, M.C. Vestergaard, H. Yoshikawa, M. Saito, E. Tamiya, Electrochemistry Communications 13 (2011) 746–749.
[30] J.Y. Cao, C. Du, S.C.C. Wang, P. Mercier, X.G. Zhang, H. Yang, D.L. Akins, Electrochemistry Communications 9 (2007) 735–740.
[31] S. Ghosh, C.R. Raj, Journal of Physical Chemistry C 114 (2010) 10843–10849.
[32] H.-P. Liang, N.S. Lawrence, L.-J. Wan, L. Jiang, W.-G. Song, T.G.J. Jones, Journal of Physical Chemistry C 112 (2008) 338–344.
[33] B.R. Rauhe, F.R. McLarnon, E.J. Cairns, Journal of Electrochemical Society 142 (1995) 1073–1084.
[34] M. Mohl, A. Kumar, A.L.M. Reddy, A. Kukovecz, Z. Konya, I. Kiricsi, R. Vajtai, P.M. Ajayan, Journal of Physical Chemistry C 114 (2010) 389–393.
[35] F. Hu, X. Cui, W. Chen, Journal of Physical Chemistry C 114 (2010) 20284–20289.
[36] L.C. Nagle, J.F. Rohan, Journal of Power Sources 185 (2008) 411–418.
[37] S.B. Newcomb, Modern approaches to the preparation of TEM samples, in: S.M.D. McVitie (Ed.), Electron Microscopy and Analysis 2003 (2004) pp. 357–362.
[38] J. Wang, X.-B. Zhang, Z.-L. Wang, L.-M. Wang, W. Xing, X. Liu, Nanoscale 4 (2012) 1549–1552.
[39] Y. Lei, B. Daffos, P.L. Taberna, P. Simon, F. Favier, Electrochimica Acta 55 (2010) 7454–7459.
[40] S.A. Sheppard, S.A. Campbell, J.R. Smith, G.W. Lloyd, T.R. Ralph, F.C. Walsh, Analyst 123 (1998) 1923–1929.
[41] M.A.V. Devanathan, M. Selvaratnam, Transactions of the Faraday Society 56 (1960) 1820–1831.
[42] M. Grden, A. Czerwinski, Journal of Solid State Electrochemistry 12 (2008) 375–385.
[43] M. Grden, J. Kotowski, A. Czerwinski, Journal of Solid State Electrochemistry 4 (2000) 273–278.
[44] Z.X. Liang, T.S. Zhao, J.B. Xu, L.D. Zhu, Electrochimica Acta 54 (2009) 2203–2208.
[45] Q.F. Yi, W. Huang, X.P. Liu, G.R. Xu, Z.H. Zhou, A.C. Chen, Journal of Electroanalytical Chemistry 619 (2008) 197–205.
[46] M.C. Jeong, C.H. Pyun, I.H. Yeo, Journal of Electrochemical Society 140 (1993) 1986–1989.
[47] T. Chierchie, C. Mayer, W.J. Lorenz, Journal of Electroanalytical Chemistry 135 (1982) 211–220.
[48] R.N. Singh, A. Singh, Anindita, International Journal of Hydrogen Energy 34 (2009) 2052–2057.
[49] R. Manoharan, J.B. Goodenough, Journal of Materials Chemistry 2 (1992) 875–887.
[50] G.W. Qin, W. Pei, X. Ma, X. Xu, Y. Ren, W. Sun, L. Zuo, Journal of Physical Chemistry C 114 (2010) 6909–6913.
[51] W. Wei, W. Chen, Journal of Power Sources 204 (2012) 85–88.
[52] C. Koenigsmann, S.S. Wong, Energy & Environmental Science 4 (2011) 1161–1176.
[53] X. Fang, L. Wang, P.K. Shen, G. Cui, C. Bianchini, Journal of Power Sources 195 (2010) 1375–1378.
[54] L. Jiang, A. Hsu, D. Chu, R. Chen, International Journal of Hydrogen Energy 35 (2010) 365–372.
[55] A.V. Tripkovic, K.D. Popovic, J.D. Momcilovic, D.M. Drazic, Journal of Electroanalytical Chemistry 448 (1998) 173–181.